

# Introducing the fission–fusion reaction process: using a laser-accelerated Th beam to produce neutron-rich nuclei towards the $N = 126$ waiting point of the $r$ -process

D. Habs · P.G. Thirolf · M. Gross · K. Allinger · J. Bin ·  
A. Henig · D. Kiefer · W. Ma · J. Schreiber

Received: 12 August 2010 / Revised version: 9 September 2010 / Published online: 16 October 2010  
© Springer-Verlag 2010

**Abstract** We propose to produce neutron-rich nuclei in the range of the astrophysical  $r$ -process (the rapid neutron-capture process) around the waiting point  $N = 126$  (Kratz et al. in Prog. Part. Nucl. Phys. 59:147, 2007; Arnould et al. in Phys. Rep. 450:97, 2007; Panov and Janka in Astron. Astrophys. 494:829, 2009) by fissioning a dense laser-accelerated thorium ion bunch in a thorium target (covered by a polyethylene layer, CH<sub>2</sub>), where the light fission fragments of the beam fuse with the light fission fragments of the target. Using the ‘hole-boring’ (HB) mode of laser radiation pressure acceleration (RPA) (Robinson et al. in Plasma Phys. Control. Fusion 51:024004, 2009; Henig et al. in Phys. Rev. Lett. 103:245003, 2009; Tajima et al. in Rev. Accel. Sci. Technol. 2:221, 2009) using a high-intensity, short pulse laser, bunches of <sup>232</sup>Th with solid-state density can be generated very efficiently from a Th layer (ca. 560 nm thick), placed beneath a deuterated polyethylene foil (CD<sub>2</sub> with ca. 520 nm), both forming the production target. Th ions laser-accelerated to about 7 MeV/u will pass through a thin CH<sub>2</sub> layer placed in front of a thicker second Th foil (both forming the reaction target) closely behind the production target and disintegrate into light and heavy fission fragments. In addition, light ions (d,C) from the CD<sub>2</sub> production target will be accelerated as well to about 7 MeV/u, also inducing the fission process of <sup>232</sup>Th in the second Th layer. The laser-accelerated ion bunches with solid-state density, which are about 10<sup>14</sup> times more dense than classically accelerated

ion bunches, allow for a high probability that generated fission products can fuse again when the fragments from the thorium beam strike the Th layer of the reaction target.

In contrast to classical radioactive beam facilities, where intense but low-density radioactive beams of one ion species are merged with stable targets, the novel fission–fusion process draws on the fusion between neutron-rich, short-lived, light fission fragments from both beam and target. Moreover, the high ion beam density may lead to a strong collective modification of the stopping power in the target by ‘snowplough-like’ removal of target electrons, leading to significant range enhancement, thus allowing us to use rather thick targets.

Using a high-intensity laser with two beams with a total energy of 300 J, 32 fs pulse length and 3 μm focal diameter, as, e.g. envisaged for the ELI-Nuclear Physics project in Bucharest (ELI-NP) (<http://www.eli-np.ro>, 2010), order-of-magnitude estimates promise a fusion yield of about 10<sup>3</sup> ions per laser pulse in the mass range of  $A = 180$ – $190$ , thus enabling us to approach the  $r$ -process waiting point at  $N = 126$ . First studies on ion acceleration, collective modifications of the stopping behaviour and the production of neutron-rich nuclei can also be performed at the upcoming new laser facility CALA (Center for Advanced Laser Applications) in Garching.

## 1 Introduction

Elements like platinum, gold, thorium and uranium are produced via the rapid neutron-capture process ( $r$ -process) at astrophysical sites like merging neutron star binaries or (core collapse) supernova type II explosions with outbursts of very high neutron density in the range of  $10^{21}$ – $10^{30}$ /cm<sup>3</sup>. We aim at improving our understanding of these nuclear

D. Habs · P.G. Thirolf (✉) · M. Gross · K. Allinger · J. Bin ·  
A. Henig · D. Kiefer  
Fakultät für Physik, Ludwig-Maximilians Universität München,  
85748 Garching, Germany  
e-mail: [peter.thirolf@physik.uni-muenchen.de](mailto:peter.thirolf@physik.uni-muenchen.de)

D. Habs · W. Ma · J. Schreiber  
Max-Planck-Institut für Quantenoptik, 85748 Garching, Germany

processes by measuring the properties of heavy nuclei on (or near) the  $r$ -process path. According to a recent report by the US National Research Council of the National Academy of Science, the origin of the heaviest elements remains one of the 11 greatest unanswered questions of modern physics [8]. While the lower path of the  $r$ -process for the production of heavy elements is well explored, the nuclei around the  $N = 126$  waiting point critically determine this element production mechanism. At present basically nothing is known about these nuclei.

Special ingredients of this proposal are: (i) the very efficient radiation pressure acceleration (RPA) mechanism for laser-based ion acceleration, especially exploiting the ‘hole-boring’ (HB) mode [4] producing pancake-like beam bunches of solid-state density; (ii) the strongly reduced stopping power of these dense bunches in a second thick Th target, where the decomposition into fission fragments and the fusion of these fragments takes place. After the laser flash we want to extract rather long-lived isotopes ( $> 100$  ms) in flight, separate them, e.g. in a (gas-filled) recoil separator and study them via decay spectroscopy or lifetime and nuclear mass measurements.

In the following we outline the relevance of the project for nuclear astrophysics and describe the new laser acceleration scheme, in particular the new fission–fusion reaction method. Finally the planned ELI-Nuclear Physics facility

will be briefly introduced, where the production of these nuclei and the experiments to measure their properties will be realized.

## 2 The relevance of the $N = 126$ waiting point for nuclear astrophysics

Figure 1 shows the nuclidic chart marked with different nucleosynthesis pathways for the production of heavy elements in the Universe: the thermonuclear fusion processes in stars producing elements up to iron (orange arrow), the slow neutron-capture process ( $s$ -process) along the valley of stability leading to about half of the heavier nuclei (red arrow) and the rapid neutron-capture process ( $r$ -process) proceeding along pathways with neutron separation energies  $S_n$  in the range of 2–3 MeV. In this scenario, rather neutron-rich nuclei are populated in an intense neutron flux [9]. The  $r$ -process path exhibits characteristic vertical regions for constant magic neutron numbers of 50, 82 and 126, where the  $r$ -process is slowed down due to low neutron-capture cross sections when going beyond the magic neutron numbers. These decisive bottlenecks of the  $r$ -process flow are called waiting points [10].

The astrophysical site of the  $r$ -process nucleosynthesis is still under debate: it may be cataclysmic core collapse su-

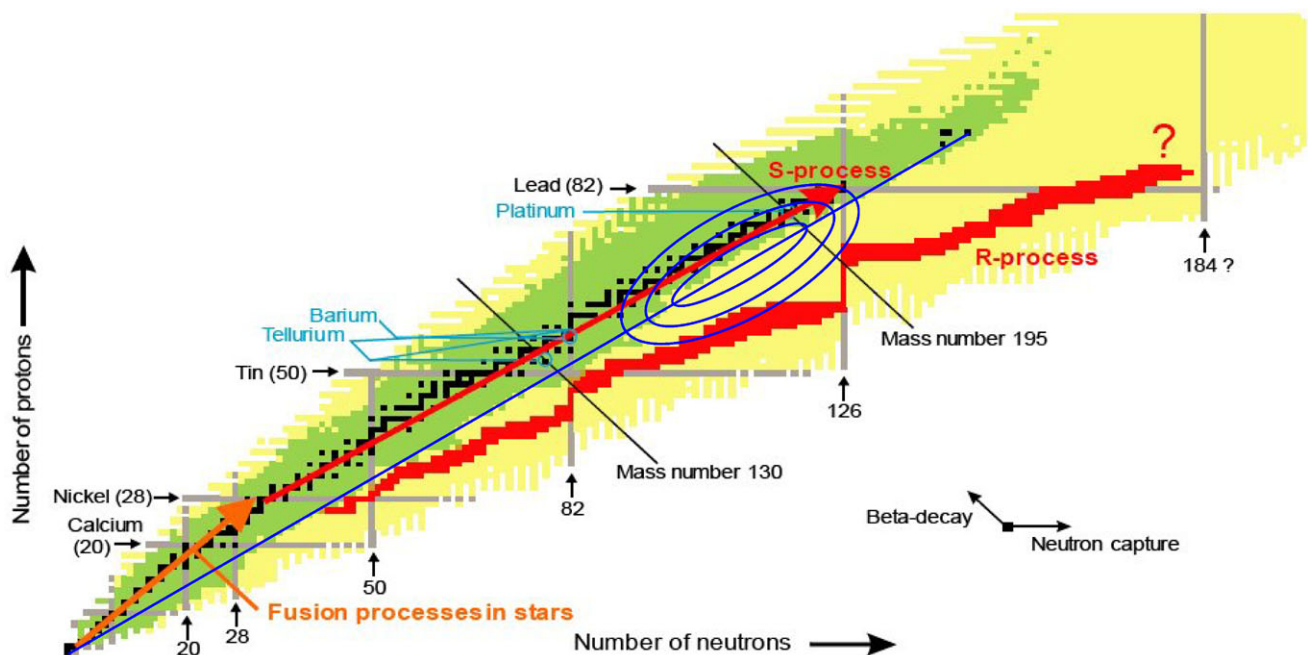


**Fig. 1** Chart of the nuclides indicating various pathways for astrophysical nucleosynthesis: thermonuclear fusion reactions in stars (orange vector),  $s$ -process path (red vector) and the  $r$ -process generating heavy nuclei in the Universe (red pathway). The nuclei marked in black indicate stable nuclei. For the green nuclei some nuclear properties are known, while the yellow, yet unexplored regions extend to the neutron

and proton drip lines. The blue line connects nuclei with the same neutron/proton ratio as for (almost) stable actinide nuclei. On this line the maximum yield of nuclei produced via fission–fusion (without neutron evaporation) will be located. The elliptical contour lines correspond to the expected maximum fission–fusion cross sections decreased to 50%, 10% and 0.1%, respectively, for primary  $^{232}\text{Th}$  beams

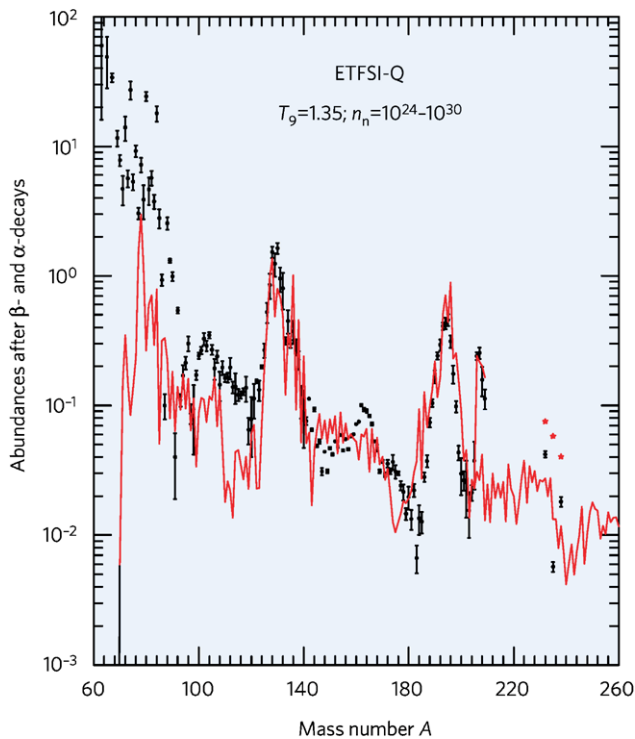


**Fig. 2** Observed elemental solar abundances in the  $r$ -process mass range (black symbols with error bars) in comparison with calculated abundances (red line and symbols), normalized to silicon =  $10^6$ . The theoretical predictions show the elemental abundances for stable isotopes after  $\alpha$  and  $\beta$  decay as obtained in the ETFSI-Q mass model [1, 16] for a wide range of neutron densities  $n_n$  (in  $1/\text{cm}^3$ ) and temperatures  $T_9$  (in units of  $10^9\text{K}$ ) and including shell quenching effects. Included with permission from [17]

pernovae (II) explosions with neutrino winds [2, 3, 11, 12] or mergers of neutron star binaries [13–15]. The  $r$ -process element abundances from galactic halo stars tell us that the  $r$ -process site for lighter and heavier neutron-capture processes may occur under different astrophysical conditions [10]. For the heavier elements beyond barium, the isotopic abundances are always very similar (called universality) and the process seems to be very robust. Perhaps also the recycling of fission fragments from the end of the  $r$ -process strengthens this stability. Presently, it seems more likely that a merger of neutron star binaries is the source for the heavier  $r$ -process branch, while core collapsing supernova explosions contribute to the lighter elements below barium. The modern nuclear equations of state, neutrino interactions and recent supernova explosion simulations [3] lead to detailed discussions of the waiting point  $N = 126$ . Here measured nuclear properties along the  $N = 126$  waiting point may help to clarify the sites of the  $r$ -process.

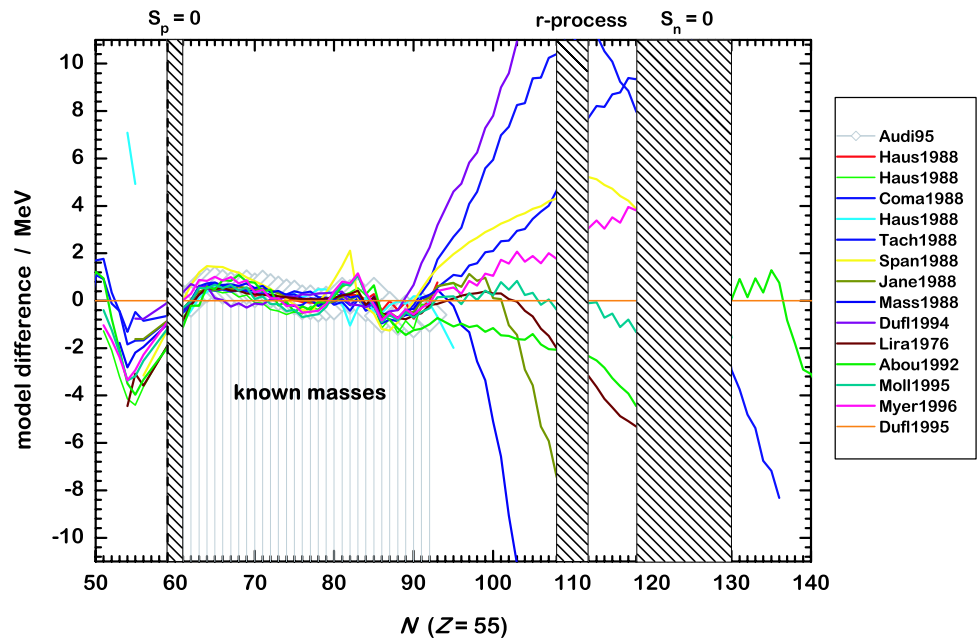
Figure 2 shows the measured solar elemental abundances of the  $r$ -process nuclei together with a calculation, where masses from the extended Thomas–Fermi plus Strutinsky integral (ETFSI) mass model [16] have been used together with several neutron flux components, characterized by a

temperature  $T_9$ , neutron densities  $n_n$  and expansion time scales. A quenching of shell effects [18] was assumed in the nuclear mass calculations to achieve a better agreement between observed and calculated abundances.

The three pronounced peaks visible in the abundance distribution seem to be of different origin, which is also reflected in the theoretical calculations shown in Fig. 2, where contributions from different temperatures and neutron densities are superimposed to the observed data. We note the pronounced third peak in the abundance distribution around  $A = 180$ – $200$ , corresponding to the group of elements around gold, platinum and osmium, where until now no experimental nuclear properties have been measured for  $r$ -process nuclei. Several astrophysical scenarios are possible to explain this third abundance peak. A detailed knowledge of nuclear lifetimes and binding energies in the region of the  $N = 126$  waiting point will narrow down the possible astrophysical sites. If, e.g. no shell quenching could be found in this mass range, the large dip existing for this case in front of the third abundance peak would have to be filled up by other processes like neutrino wind interactions. For cold decompressed neutron-rich matter, e.g. from neutron star mergers, we find an equilibrium between  $(n, \gamma)$  and  $\beta$  decay. For the rather hot supernova explosion scenario we find an equilibrium between  $(n, \gamma)$  and  $(\gamma, n)$  reactions. Considering the still rather large difficulties in identifying convincing astrophysical sites for the third peak of the  $r$ -process with sufficient occurrence rates, measurements of the nuclear properties around the  $N = 126$  waiting point will represent an important step forward in solving the difficult and yet confusing site selection of the third abundance peak of the  $r$ -process.

The key bottleneck nuclei of the  $N = 126$  waiting point around  $Z \approx 70$  are about 15 neutrons away from presently known nuclei (see Fig. 1), with a typical drop of the production cross section for classical radioactive beam production schemes of about a factor of 10–20 for each additional neutron towards more neutron-rich isotopes. Thus presently nothing is known about these nuclei, and even next-generation large-scale ‘conventional’ radioactive beam facilities like FAIR [19], SPIRAL II [20] or FRIB [21] will not be able to grant experimental access to the most important isotopes on the  $r$ -process path. The third peak in the abundance curve of  $r$ -process nuclei is due to the  $N = 126$  waiting point as visible in Fig. 1. These nuclei are expected to have rather long half-lives of a few hundred milliseconds. This waiting point represents the bottleneck for the nucleosynthesis of heavy elements up to the actinides. From the viewpoint of astrophysics, it is in the last region where the  $r$ -process path is close to the valley of stability and thus can be studied with the new isotopic production scheme discussed below. While the waiting point nuclei at  $N = 50$  and  $N = 82$  have been studied rather extensively [22–25], nothing is known experimentally about the nuclear properties of

**Fig. 3** Differences between nuclear mass predictions from various theoretical mass models for Cs isotopes ( $Z = 55$ ) compared to measured masses taken from AME95 [26] as a function of the neutron number  $N$  (for  $Z = 55$ ). The figure is taken with permission from [25]



waiting point nuclei at the  $N = 126$  magic number. Nuclear properties to be studied here are nuclear masses, lifetimes,  $\beta$ -delayed neutron emission probabilities  $P_{\nu,n}$  and the underlying nuclear structure.

For the overall description of the  $r$ -process, the nuclear masses are typically taken from mass models like the macroscopic-microscopic finite range droplet model (FRDM). Alternatively, models more closely related to first principles like Hartree–Fock–Bogoliubov calculations are used [2, 10]. Typically, somewhat less shell quenching is assumed for the heavier  $N = 126$  region compared to the  $N = 82$  region of the  $r$ -process.

Figure 3 displays the difference between nuclear masses for the isotopic chain  $Z = 55$  (Cs) as calculated by various mass models and measured masses (data taken from AME95 [26]). The plot demonstrates the good agreement between measured and predicted masses in the mass range where experimental data are available, while drastic deviations occur outside these regions and especially for the  $r$ -process region [25]. For the Cs isotopes with  $Z = 55$  as shown in Fig. 3 the mass measurements closely approach the  $r$ -process path. However, for the heavier elements relevant for the  $r$ -process waiting point  $N = 126$  around  $Z \approx 70$ , the known isotopes are about 15 neutrons away from the magic neutron number  $N = 126$ , and Fig. 3 impressively illustrates the extremely large uncertainties presently expected for any theoretical prediction of nuclear masses,  $Q$  values or  $\beta$  half-lives which may partly be attributed to effects of nuclear deformation. This clearly points to the importance of direct measurements in this mass region, especially targeting nuclear masses.

Moreover, presently there exist difficulties in describing consistently the third abundance peak of the  $r$ -process, the

$^{232}\text{Th}$  and  $^{238}\text{U}$  cosmochronometers and the potential ‘fission cycle’ beyond  $A > 260$  [27].

From the viewpoint of nuclear structure theory, semi-magic, heavy nuclei not too far away from stability are spherical and thus can generally be treated more successfully than heavy deformed nuclei. Shell model calculations with open proton and neutron shells require extremely large dimensions of the configuration space. With realistic density functional theories, some extremely time-consuming deformed RPA calculations with Skyrme or Gogny forces have been performed [28], but still spherical nuclei can be controlled much better. Also the subsystem of neutrons or protons allows us to study systems with large isospin. These density functional calculations have to be fitted to experimental data of heavy nuclei, in order to enable reliable predictions for other nuclei [28]. If we improve our experimental understanding of this final bottleneck to the actinides at  $N = 126$ , many new visions open up: (i) For many mass formulas (e.g. [29]), there is a branch of the  $r$ -process leading to extremely long-lived superheavy elements beyond  $Z = 110$  with lifetimes of about  $10^9$  years. If these predictions could be made more accurate, a search for these superheavy elements in nature would become more promising. (ii) At present the prediction for the formation of uranium and thorium elements in the  $r$ -process is rather difficult, because there are no nearby magic numbers and those nuclei are formed during a fast passage of the nuclidic area between shells. Such predictions could be improved if the bottleneck of actinide formation were more reliably known. (iii) One could also clarify the question of whether fission fragments are recycled in many  $r$ -process loops or if only a small fraction is reprocessed.



This description of our present understanding of the  $r$ -process underlines the importance of the present project for nuclear physics and, particularly, for astrophysics.

### 3 The fission–fusion reaction process

In the following section the various ingredients enabling the new fission–fusion reaction scenario are outlined. First the RPA method of laser ion acceleration is described with special emphasis on the HB mode, which allows us to generate ultra-dense ion beams. Consequently, collective effects are expected for the interaction of these ion beams with solid targets, leading to a significant reduction of the conventional electronic stopping power. Finally, the fission–fusion reaction process based on these ultra-dense laser-accelerated ion beams is described, and an order-of-magnitude estimate for the achievable fusion yield is presented.

#### 3.1 Laser ion acceleration

Laser-accelerated energetic ion beams have been produced during the last few years from micrometre thick metallic foils when irradiated by ultra-intense, short laser pulses [30–32]. In these experiments the high-energy electrons produced at the front of the target penetrated the target being opaque to the laser. At the rear side the electrons generate an electrostatic field, which ionizes and accelerates ions from the rear side. This acceleration mechanism was called target normal sheath acceleration (TNSA). It was explored in many experiments at various high-intensity laser laboratories [33–36]. A recent review [37] shows that the ion energy scales proportional to the square root of the laser intensity. Typical conversion efficiencies from laser energy to ion energy amount to less than 1%.

In the proposal of the new nuclear reaction scenario in this work, we envisage to exploit instead the new radiation pressure acceleration (RPA) mechanism for ion acceleration. It was first proposed theoretically [4, 38–41]. Special emphasis has been given to RPA with circularly polarized laser pulses, as this suppresses fast electron generation and leads to the interaction dominated by the radiation pressure [4, 38]. It has been shown that RPA operates in two modes. In the first one, called ‘hole-boring’ (HB), the laser pulse interacts with targets thick enough to allow it to drive target material ahead of it as a piston, but without interacting with the target rear surface [4].

An alternative scenario, called the ‘light-sail’ (LS) mode of RPA, occurs if the target is sufficiently thin for the laser pulse to punch through the target and accelerate part of the plasma as a single object [39, 40]. Typically the HB mode leads to lower velocities of the accelerated ions, as envisaged for the present proposal.

The first experimental observation of RPA in the HB regime was achieved only recently in experiments led by the Munich group [5, 6].

The RPA laser ion acceleration mechanism in general provides a much larger efficiency for the conversion from laser energy to ion energy and allows for a generation of much larger ion energies in comparison to TNSA. Moreover, for circularly polarized laser light RPA holds promise of quasi-monoenergetic ion beams. Due to the circular polarization, electron heating is strongly suppressed. The electrons are compressed to a dense electron sheet in front of the laser pulse, which then accelerates the ions via the Coulomb field. This mechanism requires much thinner targets and ultra-high contrast laser pulses to avoid the pre-heating and expansion of the target before the interaction with the main laser pulse.

The RPA mechanism allows us to produce ion bunches with solid-state density ( $10^{22}$ – $10^{23}/\text{cm}^3$ ), which thus are  $\approx 10^{14}$  times more dense than ion bunches from classical accelerators. Correspondingly, the areal densities of these bunches are  $\approx 10^7$  times larger. It is important to note that these ion bunches are accelerated as neutral ensembles together with the accompanying electrons and thus do not Coulomb explode.

For an estimate of the required laser intensities, focal spot area and target thickness, the 1-D RPA model as outlined in [4] is sufficient. It holds true for the relativistic HB regime of RPA. For the achievable ion energy  $E_i$  it yields the expression (circular polarized light)

$$E_i = E_u \cdot A = 2m_i c^2 \mathcal{E} / (1 + 2\sqrt{\mathcal{E}}), \quad (1)$$

where  $E_u$  is the energy per nucleon,  $A$  is the atomic mass number,  $m_i$  is the ion mass,  $c$  is the vacuum speed of light, and  $\mathcal{E}$  is the dimensionless pistonioning parameter given by

$$\mathcal{E} = I_L / (m_i n_i c^3). \quad (2)$$

$I_L$  denotes the laser intensity and  $n_i$  the ion density. In the non-relativistic limit  $\mathcal{E} \ll 1$ , (1) reduces to  $E_i = 2m_i c^2 \mathcal{E}$ , which together with (2) is equivalent to Macchi’s equation (1) in [38]. The conversion efficiency of laser energy to ion energy,  $\chi$ , follows from [4]

$$\chi = 2\sqrt{\mathcal{E}} / (1 + 2\sqrt{\mathcal{E}}). \quad (3)$$

The total number of ions,  $N_i$ , that can be accelerated results from the energy balance

$$N_i E_i = \chi W_L, \quad (4)$$

where  $W_L$  denotes the energy of the laser pulse.

The target arrangement we want to use is depicted in Fig. 4. It actually consists of two targets termed production

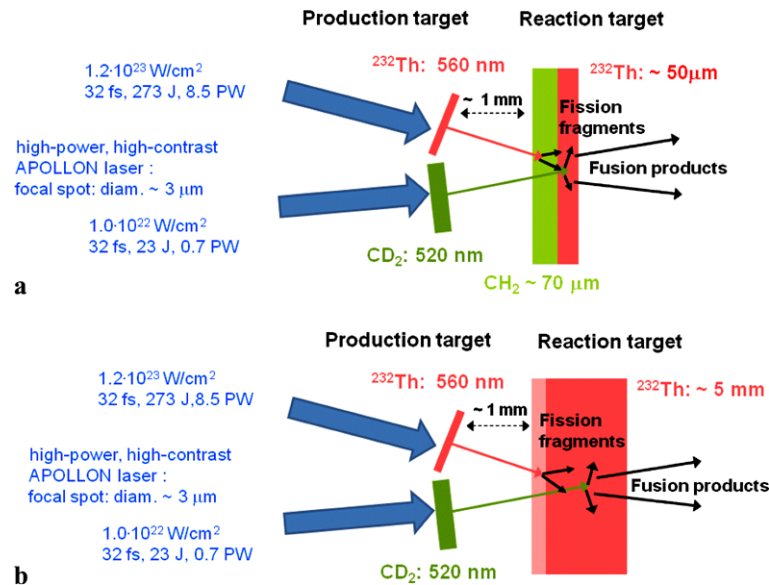


**Fig. 4** Sketch of the target arrangement envisaged for the fission–fusion reaction process based on laser ion acceleration. Part (a) illustrates the situation in the case where no collective effects on the electronic stopping are taken into account. In this case the thickness of the  $\text{CH}_2$  layer as well as the second thorium reaction target have to be limited to  $70 \mu\text{m}$  and  $50 \mu\text{m}$ , respectively, in order to enable fission of beam and target nuclei. This will allow for fusion between their light fragments as well as enable the fusion products to leave the second

thorium reaction target. Part (b) depicts an alternative scenario, where we also consider collective effects in the reaction target induced by the ultra-dense ion bunches. Here the first part of the thorium reaction target is used to decelerate the fission fragments from about  $7 \text{ MeV/u}$  to about  $3 \text{ MeV/u}$ , suitable for efficient fusion of neutron-rich species. Due to the reduced electronic stopping, a larger target thickness and thus increased fission and fusion yields can be expected. Further details are discussed in the text

target and reaction target. The first is composed of two spatially separated foils, one made from thorium and the other from deuterated polyethylene,  $\text{CD}_2$ . They serve for the generation of a thorium ion beam and a beam containing carbon ions and deuterons. The reaction target has a sandwich structure. The first layer is made from  $\text{CH}_2$  and causes fission of the accelerated thorium nuclei. The second layer is a pure thorium film. The accelerated carbon ions and deuterons lead to fission of these thorium nuclei. Fusion of the fragments created in both layers generates neutron-rich nuclei in a mass range towards the waiting point  $N = 126$ . This reaction scheme works best when the thorium and carbon ions and the deuterons each have the energy of  $7 \text{ MeV}$  per nucleon (for details see Sect. 3.2 and the following sections).

Accelerating  $^{232}\text{Th}$  ions whose density  $\rho_{\text{Th}} = m_{\text{Th}} n_{\text{Th}}$  amounts to  $11.7 \text{ g/cm}^3$  to  $E_u = 7 \text{ MeV}$  per nucleon with laser light of  $0.8 \mu\text{m}$  wavelength requires, according to (1) and (2), an intensity of  $1.2 \times 10^{23} \text{ W/cm}^2$ . The dimensionless vector potential,  $a_L$ , follows from

$$a_L = \sqrt{\frac{f \cdot I_L [\text{W cm}^{-2}] \cdot \lambda_L^2 [\mu\text{m}^2]}{1.37 \times 10^{18}}} \quad (5)$$

with  $f = 1$  for linear and  $f = 1/2$  for circular polarized light, respectively. Equation (5) gives the value of 167 for  $1.2 \times 10^{23} \text{ W/cm}^2$  and  $\lambda_L = 0.8 \mu\text{m}$ , at circularly polarized light. The conversion efficiency,  $\chi$ , reaches 11% ( $\mathcal{E} =$

$3.8 \times 10^{-3}$ ). Intensities of this level will be achievable with the APOLLON facility, which is under development at the ENSTA/Ecole Polytechnique in Palaiseau within the ILE project [47] and will form the backbone of the ELI-Nuclear Physics project. The APOLLON single-beam pulses will provide  $W_L = 150 \text{ J}$  in  $t_L = 32 \text{ fs}$ , corresponding to  $4.7 \text{ PW}$ . The sum of two of these beams is assumed to be available for the present estimate. Because of  $W_L = I_L \cdot A_F \cdot t_L$  these values fix the focal spot area on the thorium production target,  $A_F$ , to  $7.1 \mu\text{m}^2$  ( $3 \mu\text{m}$  diameter) and, from (4) the number of accelerated thorium ions,  $N_i$ , to  $1.2 \times 10^{11}$ . The thickness of the thorium foil,  $d_{\text{Th}}$ , follows from  $N_i = A_F d_{\text{Th}} n_{\text{Th}}$  and amounts to  $560 \text{ nm}$  ( $n_{\text{Th}} = 3 \times 10^{22} / \text{cm}^3$ ).

The data for the  $\text{CD}_2$  case is obtained similarly. As shown in [42], the carbon ions and deuterons will experience the same energy per nucleon. The pistoning parameter and the conversion efficiency have hence the same values as before,  $\mathcal{E} = 3.8 \times 10^{-3}$  and  $\chi = 0.11$ . Equation (2) then yields  $1.0 \times 10^{22} \text{ W/cm}^2$  ( $a_L = 48$ ) for the focal intensity,  $I_L$ , whereby for the polyethylene density,  $\rho_{\text{PE}} = m_c n_c + m_d n_d$ , the value of  $1 \text{ g/cm}^3$  is taken. Assuming here again a focal spot diameter of  $3 \mu\text{m}$  ( $A_F = 7.1 \mu\text{m}^2$ ), the required laser energy,  $W_L = I_L A_F t_L$ , results in  $23 \text{ J}$ . The number of accelerated carbon ions and deuterons amounts to  $1.4 \times 10^{11}$  and  $2.8 \times 10^{11}$ , respectively. The thickness of the polyethylene foil,  $d_{\text{PE}}$ , is  $520 \text{ nm}$ .

Phase-stable acceleration [45, 46] would yield monochromatic ion energy spectra. Whether this can be really achieved, in particular when several ion components with different charge-to-mass ratios are present, is hardly predictable on the basis of current experimental and theoretical knowledge on ion acceleration. So for a safe evaluation of the fusion process of the thorium fragments, the ion spectra are assumed to be broad (see Sect. 3.3).

Predictions related to the important question of the beam stability based on 2-D or 3-D simulations show that plane foils heavily expand and break up due to the Rayleigh–Taylor instability [43]. Promising counter-measures include targets adequately modulated in density and shape [44, 45].

### 3.2 Stopping power for dense ion bunches in a solid target

In nuclear physics the Bethe–Bloch formula [48] is used to calculate the atomic stopping of energetic individual ions

$$-\frac{dE}{dx} = 4\pi n_e \frac{Z_{\text{eff}}^2 e^4}{m_e v^2} \left[ \ln \left\{ \frac{2m_e v^2}{I_p (1 - (v/c)^2)} \right\} - \left( \frac{v}{c} \right)^2 \right], \quad (6)$$

where  $I_p$  denotes the ionization potential,  $n_e$  the electron density, and  $m_e$  the mass of the electron, while  $v$  is the ion velocity and  $Z_{\text{eff}}$  is the effective charge of the ions.

For laser-accelerated ions the ion bunch densities reach solid-state density, which is about 14 orders of magnitude larger compared to beams from classical accelerators. In such a scenario collective effects become important. According to [49], the Bethe–Bloch equation can be decomposed into a first part describing binary collisions and a second term describing long-range collective contributions according to

$$-\frac{dE}{dx} = 4\pi n_e \frac{Z_{\text{eff}}^2 e^4}{m_e v^2} \left[ \ln(m_e v^2 / e^2 k_D) + \ln(k_D v / \omega_p) \right]. \quad (7)$$

Here  $k_D$  is the Debye wave number and  $\omega_p$  is the plasma frequency of the electrons. In [50] the mechanism of collective deceleration of a dense particle bunch in a thin plasma is discussed, where the particle bunch fits into a half of one plasma oscillation and is decelerated  $10^5$ – $10^6$  times stronger than predicted by the classical Bethe–Bloch equation [48] due to a strong collective wakefield. Now we discuss the opposite effect with a strongly reduced atomic stopping power that occurs when sending the energetic, solid-state density ion bunch into a solid carbon or thorium target. For this target the plasma wavelength ( $\lambda_p \approx 5$  nm, driven by the ion bunch with a phase velocity corresponding to the thorium ion velocity) is much smaller than the ion bunch length ( $\approx 560$  nm), and collective acceleration and deceleration effects cancel. Only the binary collisions remain and contribute to the stopping power. Hence, we may

consider the dense ion bunch as consisting of about 1750 atomic layers with a distance between the Th ions of about 3.2 Å as obtained from the bulk density of metallic thorium ( $11.7 \text{ g/cm}^3$ ). In this case the first layers of the ion bunch will attract the electrons from the target and, like a snowplough, will take up the decelerating electron momenta. Hence the predominant part of the ion bunch is screened from electrons, and we expect a drastic reduction of the stopping power. The electron density  $n_e$  will be strongly reduced in the channel defined by the laser-accelerated ions, because many electrons are expelled by the ion bunch and the laser pulse. This effect requires detailed experimental investigations planned for the near future, aiming at verifying the perspective to use a significantly thicker reaction target. The classical ion range for, e.g., 7 MeV/u thorium ions in carbon is  $15 \text{ mg/cm}^2$ , corresponding to a range of 66 μm, while this range amounts to only 40 μm in a thorium target. However, if we aim at limiting the usable effective range to a thorium target thickness where the remaining projectile energy is still sufficient to induce fission, using the accelerated thorium ions directly to induce fission in the Th target would result in a usable target range of less than 10 μm without invoking collective effects. However, the use of proton-induced fission leads to a usable target thickness of about 50 μm.

The expected reduced atomic stopping power will be supported by the strong laser heating of the electrons. A reduction of the atomic stopping is essential to avoid a strong slowing down of the ions below the Coulomb barrier energies, where nuclear reactions are no longer possible. However, even without this reduced stopping power the basic properties of the novel reaction mechanism could still be studied, but with significantly reduced yields.

Taking collective effects into account by assuming a range enhancement by a factor of 100, we expect a usable thickness of several millimetres for a thorium target.

An optimized ion acceleration scheme will depend on measured stopping powers of the dense bunches in targets of different materials and thicknesses, including the ion beam energy as a further parameter to be optimized in preparatory studies.

### 3.3 The fission–fusion process

The basic concept of the fission–fusion reaction scenario draws on the ultra-high density of laser-accelerated ion bunches. Choosing fissile isotopes as target material for a first target foil accelerated by an intense laser pulse will enable the interaction of a dense beam of fission fragments with a second target foil also consisting of fissile isotopes. Thus finally in a second step of the reaction process, fusion between (neutron-rich) beam-like and target-like fission products will become possible, generating extremely neutron-rich ion species.

For our discussion we choose  $^{232}\text{Th}$  (the only component of chemically pure Th) as the fissile target material, primarily because of its long half-life of  $1.4 \times 10^{10}$  years, which avoids extensive radioprotection precautions during handling and operation. Moreover, metallic thorium targets are rather stable in a typical laser vacuum of  $10^{-6}$  mbar, whereas e.g. metallic  $^{238}\text{U}$  targets would quickly oxidize. Nevertheless, in a later stage it may become advantageous to also use heavier actinide species in order to allow for the production of even more exotic fusion products.

In general, the fission process of the two heavy Th nuclei from beam and target will be preceded by a deep inelastic transfer of neutrons between the inducing and the fissioning nuclei. Here the magic neutron number in the superdeformed fissile nucleus with  $N = 146$  [51, 52] may drive the process towards more neutron-rich fissioning nuclei, because the second potential minimum acts like a doorway state towards fission. Since in the subsequent fission process the heavy fission fragments keep their  $A$  and  $N$  values [53], these additional neutrons will show up in the light fission fragments and assist in reaching more neutron-rich nuclei. This process will be of particular importance in the reaction scenario discussed in Sect. 3.3.2 for the case of collectively reduced stopping in the reaction target.

Figure 4 shows a sketch of the proposed fission–fusion reaction scenario for two different situations, (a) for the case of normal electronic stopping as described by the Bethe-Bloch equation and (b) for the case of reduced stopping due to collective effects in the target induced by the ultra-dense ion beam discussed earlier. The latter scenario will be discussed later.

As mentioned before, the accelerated thorium ions are fissioned in the  $\text{CH}_2$  layer of the reaction target, whereas the carbon ions and deuterons generate thorium fragments in the thick thorium layer of the reaction target. This scenario is more efficient than the one where fission would be induced by the thorium ions only.

For practical reasons we propose to place the reaction target about 1 mm behind the production target, as indicated in Fig. 4.

### 3.3.1 Induced fission with normal electronic stopping

In the scenario where the earlier discussed collective effects in the target are not taken into account (marked with (a) in Fig. 4), the thorium layer of the reaction target would have a thickness of about  $50 \mu\text{m}$ .

Using a distance of  $2.8 \text{ \AA}$  between atoms in solid layers of  $\text{CH}_2$ , the accelerated light ion bunch ( $1.4 \times 10^{11}$  ions) corresponds to 1860 atomic layers in the case of a  $520 \text{ nm}$  thick  $\text{CD}_2$  target. In order to allow for an optimized fission of the accelerated Th beam, the thicker Th layer of the reaction target, which is positioned behind the production target, is covered by about  $70 \mu\text{m}$  of polyethylene. This layer

serves a twofold purpose. Primarily it is used to induce fission of the impinging Th ion beam, generating the beam-like fission fragments. Here polyethylene is advantageous compared to a pure carbon layer because of the increased number of atoms able to induce fission on the impinging Th ions. In addition, the thickness of this  $\text{CH}_2$  layer has been chosen such that the produced fission fragments will be decelerated to a kinetic energy which is suitable for optimized fusion with the target-like fission fragments generated by the light accelerated ions in the Th layer of the reaction target, minimizing the amount of evaporated neutrons. After each laser shot, a new double-target has to be rotated into position.

In order to estimate the fission cross sections of both the beam and target nuclei, we apply geometrical considerations based on the involved nuclear radii, which can be expressed for mass number  $A$  in the usual way as

$$R = 1.2 \cdot (A)^{1/3} \text{ fm.} \quad (8)$$

Neglecting the influence of surface diffuseness effects, the resulting fission cross section of the  $^{232}\text{Th}$  beam in the  $\text{CH}_2$  layer of the reaction target amounts to  $\sigma_{\text{fis}} = \pi(R_1 + R_2)^2 = 350 \text{ fm}^2 = 3.5 \times 10^{-28} \text{ m}^2$  (3.5 b). Correspondingly, the deuteron-induced fission in the Th reaction target occurs with a cross section of about  $247 \text{ fm}^2 = 2.47 \times 10^{-28} \text{ m}^2$  (2.47 b). If we use the atomic distance of  $3.2 \text{ \AA}$  for thorium, we conclude a fission probability of about  $4.1 \times 10^{-9}$  per atomic layer.

In order to estimate the required thickness of the  $\text{CH}_2$  front layer of the reaction target, we have to take into account the range of the  $7 \text{ MeV/u}$   $^{232}\text{Th}$  ions, which is about  $120 \mu\text{m}$ . However, after  $70 \mu\text{m}$  the kinetic energy of the Th ions has already dropped to  $3 \text{ MeV/u}$ , which is about the energy required for the resulting fission fragments during the subsequent fusion step. Therefore, we estimate the thickness of the polyethylene layer to about  $70 \mu\text{m}$ , which corresponds to  $\sim 2.5 \times 10^5$  atomic layers. Together with the above estimated fission probability per atomic layer and considering that from  $\text{CH}_2$  three atoms will contribute to the fission process of the impinging Th beam, this results in a fission probability for the Th ion beam of about  $3.1 \times 10^{-3}$  in the  $70 \mu\text{m}$   $\text{CH}_2$  layer, thus generating about  $3.7 \times 10^8$  beam-like fission fragments per laser pulse.

The 99.7% of Th beam ions passing through the  $\text{CH}_2$  layer will enter the Th layer of the reaction target with about  $2.4 \text{ MeV/u}$ , corresponding to a range of  $21 \mu\text{m}$ . In the first atomic layers a fraction of them will undergo fission before being slowed down too much; however, the resulting fragment energies will not be suitable for the fusion step. A quantitative assessment of this component would require detailed simulations and will be finally addressed by experimental studies.

In general, the fission process proceeds asymmetrically [53]. The heavy fission fragment for  $^{232}\text{Th}$  is centred at



$A = 139.5$  (approximately at  $Z = 54.5$  and  $N = 84$ ) close to the magic numbers  $Z = 50$  and  $N = 82$ . Accordingly, the light fission fragment mass is adjusted to the mass of the fixed heavy fission fragment, thus resulting for  $^{232}\text{Th}$  in  $A_L = 91$  with  $Z_L \approx 37.5$ . During the fission process of  $^{232}\text{Th}$  for low excitation energies, typically 1.6 neutrons are emitted. However, for the discussion presented here we neglect this loss of neutrons, because 4 or 5 neutrons may be transferred to the fissioning nucleus in the preceding transfer step (particularly efficient and thus important in case of the Th-induced fission discussed in the following section). The full width at half-maximum (FWHM) of the light fission fragment peak is typically  $\Delta A_L = 14$  mass units, the 1/10 maximum width about 22 mass units [53].

So far we have considered the fission process of beam-like Th nuclei in the  $\text{CH}_2$  layer of the reaction target. Similar arguments can be invoked for the deuteron- (and carbon-) induced generation of (target-like) fission products in the subsequent thicker thorium layer of the reaction target, where deuteron- and carbon-induced fission will occur in the  $^{232}\text{Th}$  layer of the reaction target. Since we can consider the  $2.8 \times 10^{11}$  laser-accelerated deuterons (plus  $1.4 \times 10^{11}$  carbon ions) impinging on the second target per laser pulse as 1860 consecutive atomic layers, we conclude a corresponding fission probability in the Th layer of the reaction target of about  $2.3 \times 10^{-5}$ , corresponding to  $3.2 \times 10^6$  target-like fission fragments per laser pulse. A thickness of the thorium layer of the reaction target of about  $50 \mu\text{m}$  could be exploited, where the kinetic proton energy would be above the Coulomb barrier to induce fission over the full target depth.

An essential effect to be taken into account is the widening of the fission fragment beam, because a kinetic energy of about 1 MeV/u is added to the fission fragments in arbitrary directions. However, the angular distribution of fission fragments from proton- (or heavy ion-) induced fission follows a  $1/\sin(\Theta)$  distribution [53] (with  $\Theta$  denoting the fragment angle with respect to the direction of the incoming beam inducing the fission process), and thus fragments are predominantly emitted in the beam direction. Consequently, a fraction of a few percent will stay within the conical volume defined by the spot diameter of the laser focus on the production target.

Due to the additional kinetic energy of about 1 MeV/u of the fission fragments in the thick reaction target, the target-like fragment volume will also expand. Here the very short bunch length of the fragment beam becomes important. The beam velocity is about 10% of the velocity of light and during the short fly-by time of the ions of only 1 fs the fission fragments of the target can only move a distance of  $1 \mu\text{m}$ , which is still small compared to the beam diameter of  $3 \mu\text{m}$ . Thus this enlargement of the target area is negligible.

In a second step of the fission–fusion scenario, we consider the fusion between the light fission fragments of the

beam and target to a compound nucleus with a central value of  $A \approx 182$  and  $Z \approx 75$ .

Again we employ geometrical arguments for an order-of-magnitude estimate of the corresponding fusion cross section. For a typical light fission fragment with  $A = 90$ , the nuclear radius can be estimated as 5.4 fm. Considering a thickness of  $50 \mu\text{m}$  for the Th layer of the reaction target that will be converted to fission fragments, equivalent to  $1.6 \times 10^5$  atomic layers, this results in a fusion probability of about  $1.8 \times 10^{-4}$ .

With this estimate for the fusion cross section, we can finally derive an order of magnitude for the final yield of fusion products generated via the presented fission–fusion process of about 1–2 fusion products per laser shot. This estimate does not yet take into account any collective effects in the target that might result in much higher fission rates and accordingly increased fusion yields as discussed in the following section.

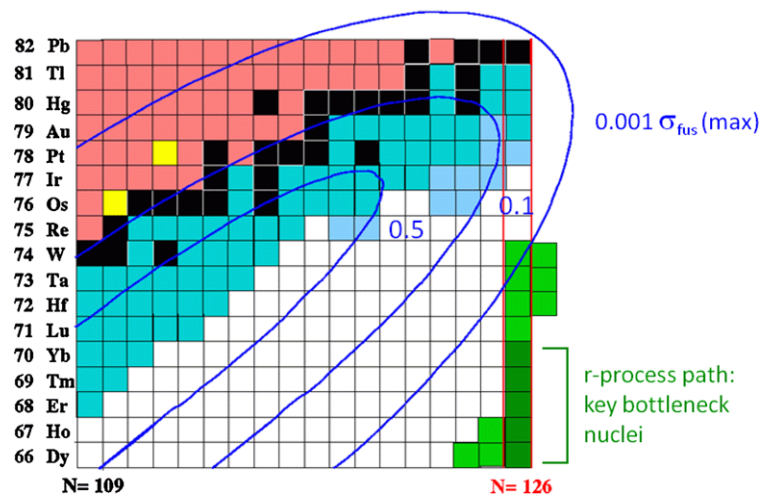
Besides the fusion of two light fission fragments, other reactions may occur. The fusion of a light fission fragment and a heavy fission fragment would lead back to the original Th nuclei, with large fission probabilities, thus we can neglect these fusion cross sections. The fusion of two heavy fission fragments would lead to nuclei with  $A \approx 278$ , again nuclei with very high fission probability. Hence we have also neglected these rare fusion cross sections, although they may be of interest on their own. Thus we concentrate here only on the fusion of two light fission fragments. Besides studying nuclei close to the waiting point of the  $r$ -process with the magic neutron number  $N = 126$ , we may also investigate neutron-rich isotopes with the magic proton number  $Z = 82$ , which are of great interest in nuclear structure studies.

Very neutron-rich nuclei still have comparably small production cross sections, because weakly bound neutrons ( $B_N \geq 3$  MeV) will be evaporated easily. The optimum range of beam energies for fusion reactions resulting in neutron-rich fusion products amounts to about 2.8 MeV/u according to PACE4 [54, 55] calculations. So, e.g. the fusion of two neutron-rich  $^{98}_{35}\text{Br}$  fission products with a kinetic energy of the beam-like fragment of 275 MeV leads with an excitation energy of about 60 MeV to a fusion cross section of 13 mb for  $^{189}_{70}\text{Yb}_{119}$ , which is already 8 neutrons away from the last presently known Yb isotope.

One should note that the well-known hindrance of fusion for nearly symmetric systems (break-down of fusion) only sets in for projectile and target masses heavier than 100 amu [56, 57]. Thus for the fusion of light fission fragments, we expect an unhindered fusion evaporation process.

In Fig. 1 the range of reachable fusion products from the fission–fusion process is indicated by the blue ellipses overlaid to the chart of nuclides. The proton to neutron ratio, which is approximately conserved during fission (indicated by the straight blue line connecting  $^1\text{H}$  with  $^{238}\text{U}$ )

**Fig. 5** Chart of nuclides around the  $N = 126$  waiting point of the  $r$ -process path. The *blue ellipses* denote the expected range of isotopes accessible via the novel fission–fusion process. The indicated *lines* represent 0.5, 0.1 and 0.001 of the maximum fusion cross section after neutron evaporation. The  $N = 126$  nuclides relevant for the  $r$ -process are marked in *green*, with the *dark green* colour indicating the key bottleneck nuclei for the astrophysical  $r$ -process



determines the slope of the inner blue elliptical contour in Fig. 1. Their eccentricity reflects the region of nuclei reachable within a range of 50% of the maximum fusion cross section, based on the large fluctuations of proton and neutron numbers of the participating fission fragments. So far the dimensions of the contour lines drawn in Figs. 1 and 5 have been estimated from usual fission distributions. Since the mass distributions of both light fission fragments exhibit a certain width (FWHM), the width of the resulting distribution after fusion will be about a factor of  $\sqrt{2}$  larger. Those distributions will steepen when reaching further out to their tails. The other two elliptical contour lines correspond to the regions of fusion products expected to be reachable with 10% and  $10^{-3}$  of the maximum cross sections, respectively.

Figure 5 displays a closer view into the region of nuclides around the  $N = 126$  waiting point of the  $r$ -process, where nuclei on the  $r$ -process path are indicated by the green colour, with dark green highlighting the key bottleneck  $r$ -process isotopes [58] at  $N = 126$  between  $Z = 66$  (Dy) and  $Z = 70$  (Yb). One should note that, e.g., for Yb, the presently last known isotope is 15 neutrons away from the  $r$ -process path at  $N = 126$ . The isotopes in light blue mark those nuclides, where recently  $\beta$ -half-lives could be measured following projectile fragmentation and in-flight separation at GSI [59]. Again the elliptical contour lines indicate the range of nuclei accessible with our new fission–fusion scenario on a level of 50%, 10% and  $10^{-3}$  of the maximum fusion cross section between two neutron-rich light fission fragments in an energy range of about 2.8 MeV/u, respectively.

### 3.3.2 Fission–fusion with collectively reduced electronic stopping

So far we estimated the expected fission and fusion yield without referring to any collective effects in the reaction targets that may reduce the electronic stopping as discussed

earlier. Now we extend this discussion by considering the expected reduction of the electronic stopping in the reaction target. This scenario would allow us to extend the thickness of the Th production target to probably a few millimetres (situation b) in Fig. 4).

While so far no experimental data or quantitative assessment on the amount of collective range enhancement is available, for the discussion within this paragraph we assume a factor of 100 and discuss the consequences.

In contrast to the previously discussed scenario without collective effects, we now propose to abandon the front carbon layer of the reaction target and use only a homogeneous, thick Th target as indicated in Fig. 4(b). In this case we use the first part of the target primarily as a stopping medium for the incoming energetic Th ions in order to decelerate them from initially about 7 MeV/u to about 3 MeV/u, which is suitable for the subsequent fusion step with target-like fragments from proton-induced fission. Since such a deceleration could be reached in about 16  $\mu\text{m}$  without collective effects, we estimate here about 0.2 mm from our 5 mm thick Th reaction target acting as a stopper while producing fission fragments too fast for efficient fusion of extremely neutron-rich isotopes. This part of the reaction target is marked by the lighter red colour in Fig. 4(b). However, this part amounts to only 4% of the reaction target and thus does not lead to a significant loss of usable fission yield. On the other hand, neutron transfer towards the deformed neutron shell closure at  $N = 146$  preceding fission will add 4 neutrons to the light fission fragment and thus significantly help to enhance fusion of very neutron-rich isotopes. Compared to the situation of Fig. 4(a), a thickness of the thorium target increased by a factor of 100 to about 5 mm due to the correspondingly reduced stopping would result in a full conversion of the Th beam into fission fragments (with  $\sim 96\%$  in an energy range usable for the fusion step). Thus  $1.2 \times 10^{11}$  beam-like light fission fragments would become available for the fusion stage of the reaction process.

Consequently the deuteron-induced fission yield in the reaction target would also rise by the same factor of 100 to a target fission probability of  $2.3 \times 10^{-3}$ . Here we use the assumption of a linear rise of the energy loss with target thickness, preserving a kinetic proton energy above the fission barrier to induce fission over the full target depth.

Thus we conclude that the expected collective stopping range enhancement will lead to a drastic increase of the fusion yield from about 1–2 fusion products per laser pulse to a value of about  $4 \times 10^4$  exotic nuclides per pulse. Most likely only part of this estimated yield enhancement could finally be realized, so it may be adequate to finally quote the average between the two extremes, resulting in an estimate of about  $10^3$  fusion products generated per laser pulse. However, it is obvious that collective effects from the ultra-dense ion bunches would significantly improve the experimental conditions towards the production of extremely neutron-rich fusion products. Moreover, if we could use a layered production target instead of the presently separated arrangement, while still achieving quasi-monoenergetic thorium and  $\text{CD}_2$  ion beams, then the primary fission fragment rates would each increase by a factor of 2, thus resulting in an increase of the fusion yield by a factor of 4.

Table 1 gives a quantitative overview of the two discussed experimental scenarios with and without collective stopping reduction, based on the parameters of the driver laser introduced earlier. All numbers refer to yields expected for one laser pulse.

**Table 1** Compilation of relevant parameters determining the expected yield (per laser pulse) of the fission–fusion reaction process proposed in this work

	Normal stopping	Reduced stopping
Production target:		
$^{232}\text{Th}$	560 nm	560 nm
$\text{CD}_2$	520 nm	520 nm
Accelerated Th ions	$1.2 \times 10^{11}$	$1.2 \times 10^{11}$
Accelerated deuterons	$2.8 \times 10^{11}$	$2.8 \times 10^{11}$
Accelerated C ions	$1.4 \times 10^{11}$	$1.4 \times 10^{11}$
Reaction target:		
$\text{CH}_2$	70 $\mu\text{m}$	–
$^{232}\text{Th}$	50 $\mu\text{m}$	5 mm
Beam-like light fragments	$3.7 \times 10^8$	$1.2 \times 10^{11}$
Target-like fission probability	$2.3 \times 10^{-5}$	$2.3 \times 10^{-3}$
Target-like light fragments	$3.2 \times 10^6$	$1.2 \times 10^{11}$
Fusion probability	$1.8 \times 10^{-4}$	$1.8 \times 10^{-4}$
Fusion products	1.5	$4 \times 10^4$

While it will remain a challenge to directly study the key waiting point isotopes on the  $r$ -process path, it is intriguing that a wide range of so far unknown isotopes will become accessible for experimental investigation.

Presently the high-intensity APOLLON laser envisaged to be used for laser ion acceleration is designed to operate at a repetition rate of one laser pulse per minute. However, laser technology is progressing rapidly with large efforts presently devoted to the development of higher repetition rates, aiming for up to 10 Hz together with an increase of the laser pulse energy beyond 1 kJ. Moreover, since the yield of very neutron-rich fusion products grows strongly nonlinear with laser energy, a final use of several coincident APOLLON laser beams would be very advantageous.

Therefore, it is foreseeable that the above given estimate for the achievable rate of neutron-rich fusion products can be increased within the next several years significantly by several orders of magnitude.

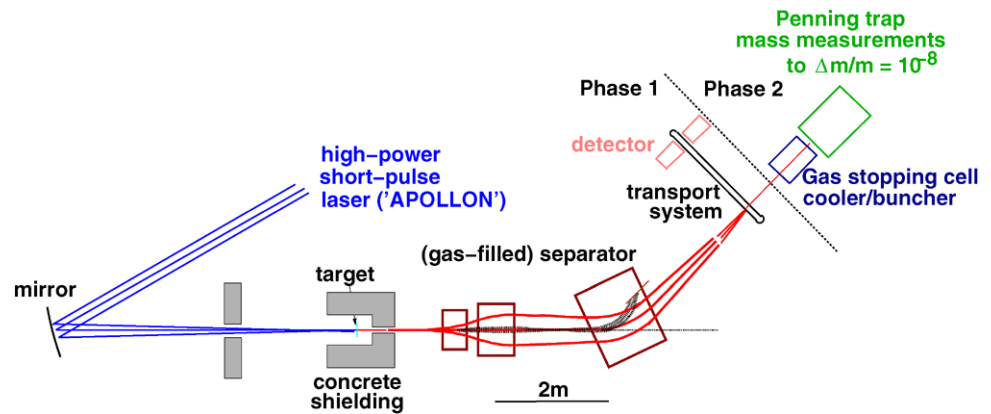
#### 4 Experimental aspects

Exploring this ‘terra incognita’ of yet unknown isotopes towards the  $r$ -process waiting point at  $N = 126$  certainly calls for a staged experimental approach. First studies should focus on the range and electronic stopping powers of dense laser-accelerated ion beams as discussed previously, followed by systematic optimizations of target properties in order to optimize the yield of fission fragments. Subsequently the  $A$ ,  $Z$  and  $N$  distributions of the light thorium fission fragments should be characterized. Moreover, it is unclear how far the first neutron transfer preceding fission will additionally broaden all these distributions. Also the yields for the fusion products should be measured in exploratory experiments, where it will be crucial to optimize the kinetic energy of the beam-like fission products.

Figure 6 shows a schematical view of the potential experimental setup of the presented reaction scenario. The high-intensity laser beam is tightly focussed onto the target assembly. This area will require heavy concrete shielding for radioprotection. Probably the most essential and also most demanding experimental task will be the separation of the reaction products. Fusion products with about 2–3 MeV/u will have to be separated from faster beam-like fission fragments with about 7 MeV/u, or target-like fragments with about 1 MeV/u, which could be achieved with a velocity filter. However, the reaction products from various fusion channels varying in mass but not in velocity require a different separation scheme. Here one could use a recoil separator (as indicated in Fig. 6), where it may be advantageous to operate the separator in gas-filled mode. Alternatively, a coarse magnetic dipole pre-separator followed by a gas stopping cell and an RFQ cooler/buncher could be used to inject

**Fig. 6** Schematic view of the experimental arrangement for fission–fusion studies.

Measurements of fusion products will be performed in two stages, first aiming at an identification of the produced isotopes via decay spectroscopy using a transport system (e.g. tape), and then later performing precision mass measurements using a Penning trap system



the ions into an electrostatic mass separator like the ‘multi-reflection time-of-flight’ mass spectrometer [60], especially when aiming for fusion products with lifetimes significantly shorter than 100 ms. Such a spectrometer could be operated either as an isobar separator or directly for mass measurements with a mass accuracy of up to  $10^{-7}$ .

In these first studies, a tape station could be used to transport the reaction products to a remote, well-shielded detector system, where the characterization of the implanted fusion products could be performed either via  $\beta$ -decay studies using, e.g.  $\text{LaBr}_3$  scintillation detectors or  $\gamma$  spectroscopy with high-resolution germanium detectors. This scenario has been labelled Phase 1 in Fig. 6. Since most of the fusion products have typical lifetimes of  $\approx 100$  ms, they will survive the transport to a secondary target and/or detector station.

In a later stage (Phase 2), the fusion products may be stopped in a buffer gas stopping cell [61, 62], cooled and bunched in, e.g., a radiofrequency quadrupole ion guide before then being transferred to a Penning trap system for high-accuracy mass measurements. Such a setup would be similar to the SHIPTRAP facility at GSI [63] or ISOLTRAP at ISOLDE/CERN [64] for mass measurement with an accuracy of  $\Delta m/m \sim 10^{-8}$ , corresponding to about 10 keV/c<sup>2</sup> [65].

## 5 Conclusion

The exploration of nuclei far away from the valley of stability is a long-term endeavour of nuclear physics with strong relevance for astrophysical applications. In our present experimental proposal of a new nuclear reaction scheme, we address the heavy nuclei of the  $r$ -process nucleosynthesis path towards the waiting point at  $N = 126$ , where our new production scheme holds promise to bring these extremely neutron-rich isotopes into reach of direct experimental studies with significantly higher yields than accessible with classical radioactive ion beam accelerator technology. With much more compact high-power, short-pulse

laser systems we intend to develop an optimized production scheme for extremely neutron-rich fusion products following induced fission from laser-accelerated ion beams. Exploiting the ‘hole-boring’ mode of the radiation pressure acceleration mechanism will allow us to generate ion beams of fissile species with solid-state density. A two-step production scheme of neutron-rich nuclides (‘fission–fusion’) is proposed, where asymmetric fission preceded by a deep inelastic transfer reaction will be followed by fusion of the light fission fragments. Moreover, collective effects reducing the electronic stopping power in the target are expected for such ultra-dense ion bunches, allowing us to use much thicker targets, thus increasing the fission yield significantly. The fusion of short-lived, neutron-rich fission fragment beams with short-lived, neutron-rich fission fragments in the target will result in very attractive production rates of extremely neutron-rich nuclides towards  $N = 126$  and  $Z > 70$ . Order-of-magnitude estimates promise fusion rates of several  $10^3$  fusion products per laser pulse, based on the laser parameters envisaged for the ELI-Nuclear Physics project in Bucharest ( $2 \times 150$  J, 32 fs). Whereas the present repetition rate of 1 laser pulse per minute limits the achievable fusion yield, ongoing development efforts for significantly higher repetition rates (aiming for up to 10 Hz) and increased laser energy (aiming for beyond 1 kJ) will open the perspective to increase the achievable yields within the fission–fusion reaction scheme by several orders of magnitude within the next several years.

In this way, high-power lasers used for laser ion acceleration can significantly contribute to access terra incognita in nuclear physics and astrophysical nucleosynthesis of heavy elements.

**Acknowledgements** We acknowledge helpful discussions with M. Heil, K.L. Kratz, H.Th. Janka and P. Ring. The authors enjoyed the collaboration with V. Zamfir, who is heading the ELI-NP project, opening up many of the new perspectives presented here. We were supported by the DFG Clusters of Excellence: ‘Munich Centre for Advanced Photonics’ (MAP) and ‘Origin and Structure of the Universe’ (UNIVERSE) and by the DFG Transregio TR18.



## References

1. K.L. Kratz, K. Farouqi, B. Pfeiffer, *Prog. Part Nucl. Phys.* **59**, 147 (2007)
2. M. Arnould, S. Goriely, K. Takahashi, *Phys. Rep.* **450**, 97 (2007)
3. I.V. Panov, H.-Th. Janka, *Astron. Astrophys.* **494**, 829 (2009)
4. A.P.L. Robinson, P. Gibbon, M. Zepf, S. Kar, R.G. Evans, C. Bellei, *Plasma Phys. Control. Fusion* **51**, 024004 (2009)
5. A. Henig, S. Steinke, M. Schnürer, T. Sokollik, R. Hörlein, D. Kiefer, D. Jung, J. Schreiber, B.M. Hegelich, X.Q. Yan, J. Meyer-ter-Vehn, T. Tajima, P.V. Nickles, W. Sandner, D. Habs, *Phys. Rev. Lett.* **103**, 245003 (2009)
6. T. Tajima, D. Habs, X. Yan, *Rev. Accel. Sci. Technol.* **2**, 221 (2009)
7. <http://www.eli-np.ro> (2010)
8. E. Haseltine, <http://discovermagazine.com/200/2feb/cover>
9. C.E. Rolfs, *Cauldrons in the Cosmos* (University of Chicago Press, Chicago, 1991)
10. K.-L. Kratz, K. Farouqi, B. Pfeiffer, J.W. Truran, C. Sneden, J.J. Cowan, *Astrophys. J.* **662**, 39 (2007)
11. H.-Th. Janka, K. Langanke, A. Marek, G. Martinez-Pinedo, B. Müller, *Phys. Rep.* **442**, 38 (2007)
12. J.J. Cowan, F.-K. Thielemann, *Phys. Today* **57**, 47 (2004)
13. C. Freiburghaus, S. Rosswog, F.-K. Thielemann, *Astrophys. J.* **525**, L121 (1999)
14. R. Surman, G.C. McLaughlin, M. Ruffert, H.-Th. Janka, W.R. Hix, *Astrophys. J.* **679**, L117 (2008)
15. K. Farouqi, C. Freiburghaus, K.-L. Kratz, B. Pfeiffer, T. Rauscher, F.-K. Thielemann, *Nucl. Phys. A* **758**, 631c (2005)
16. J.M. Pearson, R.C. Nayak, S. Goriely, *Phys. Lett. B* **387**, 455 (1996)
17. J.J. Cowan, C. Sneden, *Nature* **440**, 1151 (2006)
18. J. Dobaczewski, H. Flocard, J. Treiner, *Nucl. Phys. A* **422**, 103 (1984)
19. FAIR, An International Accelerator Facility for Beams of Ions and Antiprotons, Baseline Technical Report GSI (2006). <http://www.gsi.defairreportsbtr.html>
20. SPIRAL II, Detailed Design Study—APD Report, GANIL (2005). <http://pro.ganil-spiral2.euspiral2what-is-spiral2apd>
21. <http://www.frib.msu.edu/aboutmsu-frib-proposal>
22. S. Baruah, G. Audi, K. Blaum, M. Dworschak, S. George, C. Guenaut, U. Hager, F. Herfurth, A. Herlert, A. Kellerbauer, H.-J. Kluge, D. Lunney, H. Schatz, L. Schweikhard, C. Yazidjian, *Phys. Rev. Lett.* **101**, 262501 (2008)
23. M. Dworschak, G. Audi, K. Blaum, P. Delahaye, S. George, U. Hager, F. Herfurth, A. Herlert, A. Kellerbauer, H.-J. Kluge, D. Lunney, L. Schweikhard, C. Yazidjian, *Phys. Rev. Lett.* **100**, 072501 (2008)
24. I. Dillmann, K.-L. Kratz, A. Wöhr, O. Arndt, B.A. Brown, P. Hoff, M. Hjorth-Jensen, U. Köster, A.N. Ostrowski, B. Pfeiffer, D. Seweryniak, J. Shergur, W.B. Walters, *Phys. Rev. Lett.* **91**, 162503 (2003)
25. K. Blaum, *Phys. Rep.* **425**, 1 (2006)
26. G. Audi, A.H. Wapstra, *Nucl. Phys. A* **595**, 409 (1995)
27. I.V. Panov, E. Kolbe, B. Pfeiffer, T. Rauscher, K.-L. Kratz, F.-K. Thielemann, *Nucl. Phys. A* **747**, 633 (2005)
28. P. Ring, Private communication (2010)
29. P. Möller, J.R. Nix, W.D. Myers, W.J. Swiatecki, *At. Data Nucl. Data Tables* **59**, 185 (1995)
30. B.M. Hegelich, B.J. Albright, J. Cobble, K. Flippo, S. Letzring, M. Paffett, H. Ruhl, J. Schreiber, R.K. Schulze, J.C. Fernandez, *Nature* **439**, 441 (2006)
31. H. Schwörer, S. Pfoth, O. Jäkel, K.-U. Amthor, B. Liesfeld, W. Ziegler, R. Sauerbrey, K.W.D. Ledingham, T. Esirkepov, *Nature* **439**, 445 (2006)
32. S. Ter-Avetisyan, M. Schnürer, P.V. Nickles, M. Kalashnikov, E. Risse, T. Sokollik, W. Sandner, A. Andreev, V. Tikhonchuk, *Phys. Rev. Lett.* **96**, 145006 (2006)
33. R.A. Snavely, M.H. Key, S.P. Hatchett, T.E. Cowan, M. Roth, T.W. Phillips, M.A. Stoyer, E.A. Henry, T.C. Sangster, M.S. Singh, S.C. Wilks, A. MacKinnon, A. Offenberger, D.M. Pennington, K. Yasuike, A.B. Langdon, B.F. Lasinski, J. Johnson, M.D. Perry, E.M. Campbell, *Phys. Rev. Lett.* **85**, 2945 (2000)
34. E. Clarke, K. Krushelnick, J.R. Davies, M. Zepf, M. Tatarakis, F.N. Beg, A. Machacek, P.A. Norreys, M.I.K. Santala, I. Watts, A.E. Dangor, *Phys. Rev. Lett.* **84**, 670 (2000)
35. A. Maksimchuk, S. Gu, K. Flippo, D. Umstadter, V.Yu. Bychenkov, *Phys. Rev. Lett.* **84**, 4108 (2000)
36. S.P. Hatchett, C.G. Brown, T.E. Cowan, E.A. Henry, J.S. Johnson, M.H. Key, J.A. Koch, A.B. Langdon, B.F. Lasinski, R.W. Lee, A.J. Mackinnon, D.M. Pennington, M.D. Perry, T.W. Phillips, M. Roth, T.C. Sangster, M.S. Singh, R.A. Snavely, M.A. Stoyer, S.C. Wilks, K. Yasuike, *Phys. Plasma* **7**, 2076 (2000)
37. L. Robson, P.T. Simpson, R.J. Clarke, K.W.D. Ledingham, F. Lindau, O. Lundh, T. McCanny, P. Mora, D. Neely, C.-G. Wahlström, M. Zepf, P. McKenna, *Nat. Phys.* **3**, 58 (2007) and refs. therein
38. A. Macchi, F. Cattani, T.V. Liseykina, F. Cornolti, *Phys. Rev. Lett.* **94**, 165003 (2005)
39. O. Klimo, J. Psikal, J. Limpouch, V.T. Tikhonchuk, *Phys. Rev. Spec. Top. Accel. Beams* **11**, 031301 (2008)
40. A.P.L. Robinson, M. Zepf, S. Kar, R.G. Evans, C. Bellei, *New J. Phys.* **10**, 013021 (2008)
41. S.G. Rykovanov, J. Schreiber, J. Meyer-ter-Vehn, C. Bellei, A. Henig, H.C. Wu, M. Geissler, *New J. Phys.* **10**, 113005 (2008)
42. A.P.L. Robinson, D.-H. Kwon, K. Lancaster, *Plasma Phys. Control. Fusion* **51**, 095006 (2009)
43. T.-P. Yu, A. Pukhov, G. Shvets, M. Chen, *Phys. Rev. Lett.* **105**, 065002 (2010)
44. M. Chen, A. Pukhov, T.P. Yu, Z.M. Sheng, *Phys. Rev. Lett.* **103**, 024801 (2009)
45. X.Q. Yan, C. Lin, Z.M. Sheng, Z.Y. Guo, B.C. Liu, Y.R. Lu, J.X. Fang, J.E. Chen, *Phys. Rev. Lett.* **100**, 135003 (2008)
46. V.K. Tripathi, C.S. Liu, X. Shao, B. Eliasson, R.Z. Sagdeev, *Plasma Phys. Control. Fusion* **51**, 024014 (2009)
47. G. Mourou, The APOLLON/ILE 10 PW laser project. [http://www.nipne.ro/eli\\_np\\_workshop/contributions.php](http://www.nipne.ro/eli_np_workshop/contributions.php)
48. S. Segré, *Nuclei and Particles*, 2nd edn. (Benjamin, London, 1977)
49. S. Ichimaru, *Basic Principles of Plasma Physics: A Statistical Approach* (Benjamin, Reading, 1973)
50. H.-C. Wu, T. Tajima, D. Habs, A.W. Chao, J. Meyer-ter-Vehn, *Phys. Rev. Spec. Top. Accel. Beams* **13**, 101303 (2010)
51. P.G. Thirolf, D. Habs, *Nucl. Phys.* **49**, 325 (2002)
52. V. Metag, *Nukleonika* **20**, 789 (1975)
53. R. Vandenbosch, J.R. Huizenga, *Nuclear Fission* (Academic Press, New York, 1973)
54. A. Gavron, *Phys. Rev. C* **21**, 230 (1980)
55. O.B. Tarasov, D. Bazin, *Nucl. Instrum. Methods B* **204**, 174 (2003)
56. A.B. Quint, W. Reisdorf, K.-H. Schmidt, P. Armbruster, F.-P. Heßberger, S. Hofmann, J. Keller, G. Münzenberg, H. Stelzer, H.-G. Clerc, W. Morawek, C.-C. Sahn, *Z. Phys. A* **346**, 119 (1993)
57. W. Morawek, D. Ackermann, T. Brohm, H.-G. Clerc, U. Gollerthan, E. Hanelt, M. Horz, W. Schwab, B. Voss, K.-H. Schmidt, F.-P. Heßberger, *Z. Phys. A* **341**, 75 (1991)
58. NRC Rare Isotope Science Assessment Committee (RISAC) *Report* (National Academies Press, Washington, 2007)
59. T. Kurtukian-Nieto, J. Benlliure, K.H. Schmidt, *Nucl. Instrum. Methods A* **589**, 472 (2008)
60. W.R. Plass, T. Dickel, U. Czok, H. Geissel, M. Petrick, K. Reinheimer, C. Scheidenberger, M.I. Yavor, *Nucl. Instrum. Methods B* **266**, 4560 (2008)

61. J.B. Neumayr, L. Beck, D. Habs, S. Heinz, J. Szerypo, P.G. Thirolf, V. Varentsov, F. Voit, D. Ackermann, D. Beck, M. Block, A. Chaudhuri, Z. Di, S.A. Eliseev, H. Geissel, F. Herfurth, F.P. Heßberger, S. Hofmann, H.J. Kluge, M. Mukherjee, G. Münzenberg, M. Petrick, W. Quint, S. Rahaman, C. Rauth, D. Rodriguez, C. Scheidenberger, G. Sikler, Z. Wang, C. Weber, W.R. Plaß, M. Breitenfeldt, G. Marx, L. Schweikhard, A.F. Dodonov, Y. Novikov, M. Suhonen, *Nucl. Instrum. Methods B* **244**, 489 (2006)
62. J.B. Neumayr, P.G. Thirolf, D. Habs, S. Heinz, V.S. Kolhinen, M. Sewtz, J. Szerypo, *Rev. Sci. Instrum.* **77**, 065109 (2006)
63. M. Block, D. Ackermann, D. Beck, K. Blaum, M. Breitenfeldt, A. Chaudhuri, A. Doemer, S. Eliseev, D. Habs, S. Heinz, F. Herfurth, F.P. Hessberger, S. Hofmann, H. Geissel, H.-J. Kluge, V. Kolhinen, G. Marx, J.B. Neumayr, M. Mukherjee, M. Petrick, W. Plass, W. Quint, S. Rahaman, C. Rauth, D. Rodriguez, C. Scheidenberger, L. Schweikhardt, M. Suhonen, P.G. Thirolf, Z. Wang, C. Weber, *Eur. Phys. J. A* **25**, 49 (2005)
64. M. Mukherjee, D. Beck, K. Blaum, G. Bollen, J. Dilling, S. George, F. Herfurth, A. Herlert, A. Kellerbauer, H.-J. Kluge, S. Schwarz, L. Schweikhard, C. Yazidjian, *Eur. Phys. J. A* **35**, 1 (2008)
65. M. Block, D. Ackermann, K. Blaum, C. Droese, M. Dworschak, S. Eliseev, T. Fleckenstein, E. Haettner, F. Herfurth, F.P. Heßberger, S. Hofmann, J. Ketelaer, J. Ketter, H.-J. Kluge, G. Marx, M. Mazzocco, Yu.N. Novikov, W.R. Plaß, A. Popeko, S. Rahaman, D. Rodriguez, C. Scheidenberger, L. Schweikhard, P.G. Thirolf, G.K. Vorobyev, C. Weber, *Nature* **463**, 785 (2010)